Templated Electrodeposition and Photocatalytic Activity of Cuprous Oxide Nanorod Arrays

ARTICLE *in* ACS APPLIED MATERIALS & INTERFACES · DECEMBER 2014

Impact Factor: 6.72 · DOI: 10.1021/am507244q · Source: PubMed

11 AUTHORS, INCLUDING:

Antony Bazan
Universidad Nacional de Ingeniería (Peru)
2 PUBLICATIONS **1** CITATION
SEE PROFILE

Maria Quintana
Universidad Nacional de Ingeniería (Peru)
13 PUBLICATIONS **557** CITATIONS
SEE PROFILE

Volodymyr V Nesterov
New Mexico Highlands University
321 PUBLICATIONS **1,401** CITATIONS
SEE PROFILE

Walter Estrada
Universidad Nacional de Ingeniería (Peru)
36 PUBLICATIONS **659** CITATIONS
SEE PROFILE

ACS APPLIED MATERIALS & INTERFACES

Research Article

www.acsami.org

Templated Electrodeposition and Photocatalytic Activity of Cuprous Oxide Nanorod Arrays

Keith M. Haynes,[†] Collin M. Perry,[†] Marlene Rivas,[§] Teresa D. Golden,[†] Antony Bazan,[‡] Maria Quintana,[‡] Vladimir N. Nesterov,[†] Seare A. Berhe,[†] Juan Rodríguez,[‡] Walter Estrada,[‡] and W. Justin Youngblood*[,†]

[†]Department of Chemistry, University of North Texas, Denton, Texas 76203, United States

[‡]Facultad de Ciencias, Universidad Nacional de Ingeniería, P.O. Box 31-139, Av. Túpac Amaru 210, Lima, Perú

[§]Department of Chemistry, University of La Verne, La Verne, California 91750, United States

Supporting Information

ABSTRACT: Cuprous oxide (Cu_2O) nanorod arrays have been prepared via a novel templated electrodeposition process and were characterized for their photocatalytic behavior in nonaqueous photoelectrochemical cells. Zinc oxide (ZnO) nanorod films serve as sacrificial templates for the in situ formation of polymer nanopore membranes on transparent conductive oxide substrates. Nitrocellulose and poly(lactic acid) are effective membrane-forming polymers that exhibit different modes of template formation, with nitrocellulose forming conformal coatings on the ZnO surface while poly(lactic acid) acts as an amorphous pore-filling material. Robust template formation is sensitive to the seeding method used to prepare the precursor ZnO nanorod films. Photoelectrochemical cells prepared from electrodeposited Cu_2O films using methyl viologen as a redox shuttle in acetonitrile electrolyte exhibit significant charge recombination that can be partially suppressed by a combination of surface passivation methods. Surface-passivated nanostructured Cu_2O films show enhanced photocurrent relative to planar electrodeposited Cu_2O films of similar thickness. We have obtained the highest photocurrent ever reported for electrodeposited Cu_2O in a nonaqueous photoelectrochemical cell.

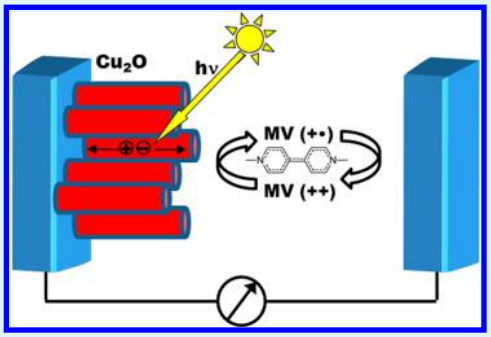

KEYWORDS: *membrane, template, electrodeposition, nanorods, cuprous oxide*

INTRODUCTION

Cuprous oxide (Cu_2O) is an instrinsic semiconductor (band gap ~2.2 eV) usually having p-type conductivity due to copper vacancies in the crystal lattice.[1−4] Cu_2O has applications in chemosensing,[5,6] photocatalysis,[7,8] photovoltaics,[9−11] and photoelectrochemical solar cells.[12−14] Technical challenges in the research and application of Cu_2O include the reliable preparation of nanostructured Cu_2O materials, the susceptibility of Cu_2O to photocorrosion,[15,16] and the adventitious formation of Cu^0 interlayers at p−n heterojunctions.[17,18] Toward the preparation of nanostructured Cu_2O, the electrodeposition of Cu_2O thin films allows the greatest control over morphology (film thickness, crystal grain size, and orientation)[19−22] and conductivity (p/n-type, dopant concentration, flat band potential, and carrier mobility),[23−28] although electrodeposited Cu_2O exhibits much lower conductivity compared to samples prepared by thermal oxidation.[29] Recent measurement of the carrier diffusion length in electrodeposited Cu_2O suggests that nanostructured Cu_2O would offer improved performance over planar films in photoelectrochemical applications.[27] Chemical bath conditions for epitaxial growth of Cu_2O nanorods from surfaces have not yet been discovered, and the annealing of Cu_2O nanoparticles into sintered mesoporous films is impractical because of the tendency of Cu_2O to oxidize to CuO when heated under ambient atmosphere,[22] or disproportionate to CuO/Cu^0 when heated under vacuum or inert atmosphere.[30,31]

We have discovered a convenient method for the preparation of vertically aligned nanorod arrays of Cu_2O on preformed electrode substrates such as transparent conductive F-SnO_2 electrodes (Figure 1). Zinc oxide (ZnO) nanorods can be used to set the morphology of a spin-cast organic polymer film. Wet-etch removal of the ZnO component enables the formation of polymer nanopore membranes onto the underlying substrate. Electrodeposition of Cu_2O from lactate-stabilized solutions of $CuSO_4$ produces aligned nanorods of Cu_2O that can be liberated from the membrane by removal of the polymer with a solvent rinse. This method provides electrodeposited nanorods with good electrical contact to the substrate and morphological fidelity to the precursor template of ZnO nanorods. A major advantage of this nanotemplating procedure is that it does not require any low-pressure vapor deposition process, and uses only an oven or water bath, a spin coater, and potentiostat. We have assessed the photoelectrochemical behavior of the as-

Received: October 22, 2014
Accepted: December 2, 2014

   dx.doi.org/10.1021/am507244q | ACS Appl. Mater. Interfaces XXXX, XXX, XXX−XXX

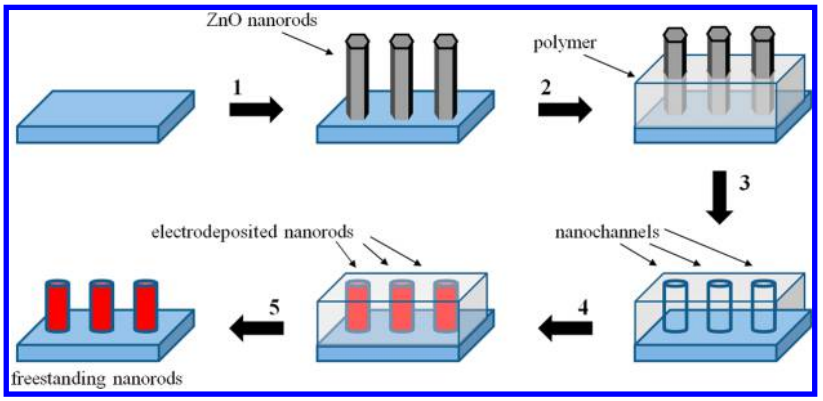

Figure 1. Process for templated electrodeposition of epitaxial nanorods onto preformed electrode substrates. **1**, ZnO nanorods are hydrothermally grown. **2**, Polymer is spin-cast from solution. **3**, ZnO is etched. **4**, Nanorod material is electrodeposited. **5**, Polymer template is removed with organic solvent.

produced Cu_2O nanorods and find that, with proper passivation of recombination sites, nanostructured films do provide higher photocurrent compared to planar films.

EXPERIMENTAL SECTION

Preparation of Nanorod Arrays. ZnO nanorods were prepared by two methods. In the first method, ZnO nanorods were seeded from MnOOH nanoparticles and grown in an aqueous bath of $ZnSO_4$, ethanolamine, and NH_4OH at 90 °C as previously reported.[32] In the second method, ZnO nanorods were seeded by spray pyrolysis of a solution of $Zn(OAc)_2$, and grown in a bath using a basic solution of $Zn(NO_3)_2$ at 90 °C.[33] Retail fingernail polish was diluted to 15% solution (v/v) in 1,2-dichloroethane/acetone (1:1). Fingernail polish is typically 13−22 wt % nitrocellulose, so the final nitrocellulose solution for spin casting is estimated at 1−2 wt % nitrocellulose.[34] Alternatively, poly(lactic acid) can be dissolved from solid to 1.5 wt % in 1,2-dichloroethane/acetone (9:1). The resulting solution was used for spin coating of ZnO nanorod films using a commercial spin coater set to 2000 rpm and run for 2 min. Polymer-coated slides were then immersed in an aqueous solution of phosphoric acid (0.5 M) or boric acid (0.5 M) and left for 5 min or overnight, respectively. Etch removal of the ZnO nanorods is apparent by the loss of light scattering in the film, with the milky-white ZnO films turning to a clear translucent film for the polymer membrane without ZnO. Nanopore membrane-coated substrates were subjected to electrodeposition using the F-SnO_2/glass substrate as a working electrode, and fitting a glass joint with an O-ring over the substrate with a clamp to make a seal. The glass vessel was filled with an aqueous solution containing lactic acid and $CuSO_4$, adjusted to pH 9 with 1 M NaOH (aq). A platinum counterelectrode and Ag/AgCl quasi reference electrode were each fitted into the vessel and wired through a septum used to seal the vessel. The electrolyte was purged with argon through the septum. The vessel was immersed in a water bath at 30 °C and electrodeposition was performed cathodically at constant potential (400−600 mV).[19]

Preparation and Testing of Photoelectrochemical Cells. Cells were assembled by melt adhesion of a thin film of Surlyn polymer between the Cu_2O/F-SnO_2 electrode and a platinized F-SnO_2 counterelectrode.[35] The cells were filled by capillary action with an electrolyte composed of 0.1 M $LiClO_4$, 50 mM methyl viologen tetrafluoroborate, and 25 mM decamethylcobaltocene. After the cells were filled with electrolyte, the entry/exit ports were sealed with Hysol 1C epoxy. Current−voltage measurements were done with a Keithley 2400 source meter and solar simulator (SolarLight, Inc.). Incident photon conversion to electron (IPCE) spectra were measured against a calibrated silicon photodiode using monochromatic light from a xenon lamp (PV Measurements QEX7).

Synthesis of 1,1′-Dimethyl-4,4′-bipyridine Bis-(tetrafluoroborate). Methyl viologen dichloride (1.08 g, 4.2 mmol) was added to 1.0 mL of water, and HBF_4 (1.60 mL of 48 wt % aqueous solution, 12.6 mmol) was added dropwise to the heterogeneous mixture. Upon addition of the acid, the beige solid turned white, and the mixture was stirred for 20 min and then filtered. The solid material was redissolved in hot water (5 mL), allowed to cool to room temperature, and stored overnight in a refrigerator at 12 °C. Colorless crystals were formed that were suitable for single-crystal X-ray diffraction. The crystals were filtered from the mother liquor, washed twice with cold ethanol, and dried in vacuo (416 mg, 28%). Analytical data, including crystal diffraction data, were consistent with previous results.[36,37]

Passivation of Cu_2O/F-SnO_2 Electrodes. Passivation with 4-nitrobenzenediazonium tetrafluoroborate was conducted as previously described.[38] Each Cu_2O/F-SnO_2 electrode was employed as the working electrode in a three-electrode cell with a platinum wire counterelectrode and a Ag/AgCl quasi reference electrode. The electrolyte was a solution of the diazonium salt (10 mM) with added tetrabutylammonium hexafluorophosphate (0.1 M) in dry acetonitrile. The cell was voltammetrically cycled between 0.2 and −0.45 V vs Ag/AgCl (quasi reference electrode in saturated KCl solution) at 0.2 V/s for 20 cycles. The cell was then disassembled and the Cu_2O/F-SnO_2 electrode was rinsed with acetonitrile, followed by ethanol, and allowed to dry in air. Passivation with TiO_2 was also conducted as previously described.[39] A solution of $(NH_4)_2TiF_6$ (50 mM) was prepared in aqueous boric acid (150 mM) and the Cu_2O/F-SnO_2 electrode was placed in the solution for 1 h. After 1 h incubation time, the electrode was removed and rinsed with deionized water and allowed to dry in air. For electrodes subjected to both passivations, the diazonium passivation was done first.

RESULTS AND DISCUSSION

Zinc oxide nanorods can be grown hydrothermally with control over diameter and height and can be etched in mild acidic or

dx.doi.org/10.1021/am507244q | ACS Appl. Mater. Interfaces XXXX, XXX, XXX−XXX

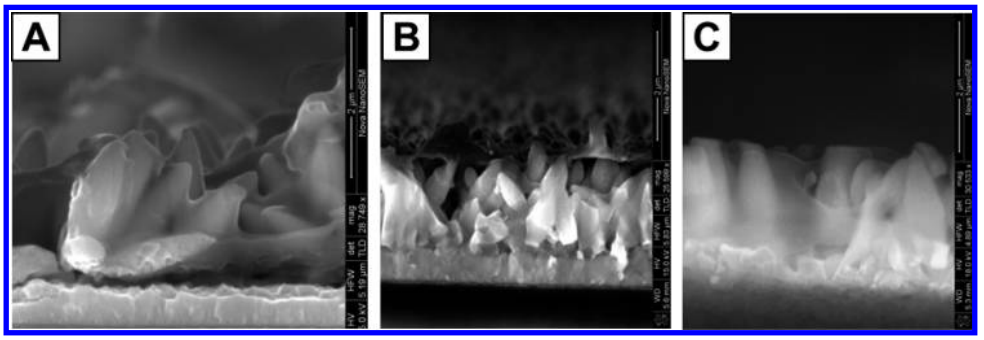

Figure 2. Polymer-coated ZnO nanorods (hydrothermally grown): (A) Nanorods coated with a single spin coat of 1−2 wt % nitrocellulose solution. (B) Nanorods coated with a single spin coat of 1.5 wt % poly(lactic acid). (C) Nanorods subjected to two rounds of spin coating with 1.5 wt % poly(lactic acid) and heat treatment on a hot plate at 200 °C for 3 min.

alkaline aqueous solution.[40] Seeding methods are preferred that provide some exposed area of the underlying substrate after nanorod growth, to promote adhesion of the membrane polymer to the substrate after removal of the oxide nanorods. ZnO nanorods seeded with nanoparticulate MnOOH provided polymer templates with good adhesion.[32] Thick ZnO seed layers prepared by spray pyrolysis or from solution-cast/annealed coatings of $Zn(OAc)_2$ result in a loose contact between the membrane and the substrate, leading to electrodeposited films with poor fidelity to the original ZnO template, and in some cases complete delamination of the polymer film occurred after ZnO etch. The template polymer must be rigid to hold the membrane shape upon removal of the ZnO nanorods. Highly viscoelastic polymers such as natural or synthetic polyisoprene ("rubber") or siloxane polymers would be unlikely to serve well in this capacity. Spin-cast solutions of nitrocellulose or poly(lactic acid) at 1−2 wt % in 1,2-dichloroethane/acetone (9:1) were effective at templating the ZnO nanorod films. A single coating of nitrocellulose adheres to the entire surface of the nanorods (Figure 2A), whereas poly(lactic acid) does not infiltrate unless melted (200 °C) after coating (Figure 2B/C). We also attempted to prepare membranes with pH-insensitive polymer materials (polystyrene and nylon-6/6) but in each case the polymer delaminated upon drying on the ZnO substrate. Upon drying, the polymer/ZnO films prepared with either nitrocellulose or poly(lactic acid) can be etched in aqueous H_2BO_3 or H_3PO_4 to provide the open-pore polymer membrane. H_3PO_4 is preferred due to its faster etching, whereas H_2BO_3 required long immersion times (>20 h) to completely remove the ZnO. Treatment with strong acids or with extremely alkaline solutions (pH >11) can distort these membranes due to partial hydrolysis and/or dissolution of the membrane. Some ZnO that is inaccessible to the etch solution persists, but cannot interfere with the electrodeposition process due to its internment within the polymer membrane. This buried ZnO is easily removed by a subsequent acid etch step after the membrane is ultimately removed, and Cu_2O is much more stable to weak and moderate acids compared to ZnO. The MnOOH seed layer is also removed during the acid etch step, as evidenced by observation that substrates coated with MnOOH nanoparticles and then treated with either H_2BO_3 or H_3PO_4 and subsequently rinsed with neutral water will not seed the growth of ZnO nanoparticles.

Cu_2O nanorods grown by potentiostatic deposition (400−600 mV negative of Ag/AgCl) from lactate-chelated aqueous $CuSO_4$ at pH 9.0 show the same diameter range as in the ZnO precursor rods, and even exhibit the hexagonal shape that was set into the template by the wurtzite ZnO nanorods (Figure 3). Cuprous oxide has a cubic crystal structure (cuprite) that generally exhibits cubic,[41] or octahedral crystal shapes.[42,43] The tips of the Cu_2O nanorods are flat unless grown to the end of the membrane pores. With nitrocellulose membranes, even large defects such as microscale ZnO rods lying on top of a bed of vertically aligned nanorods can be faithfully reproduced (see

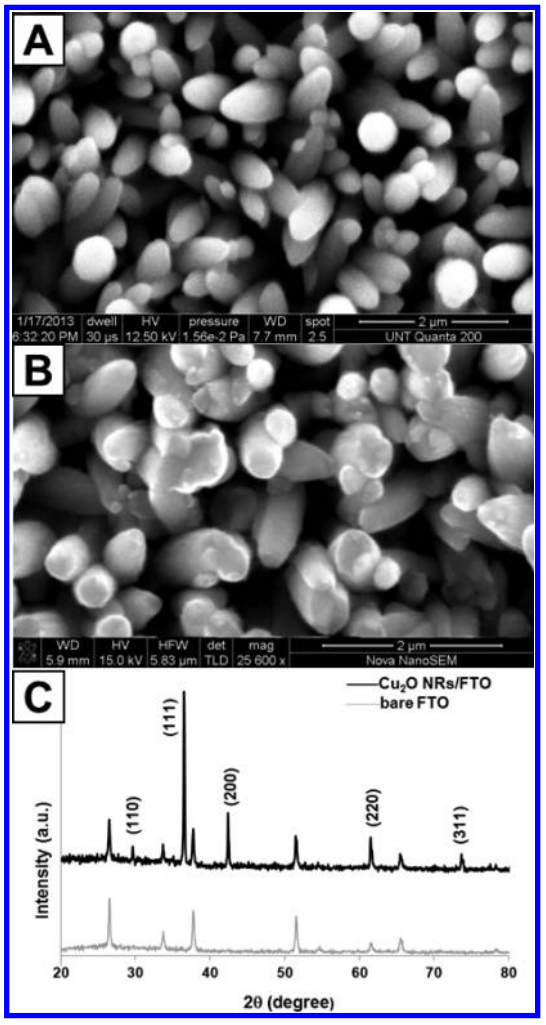

Figure 3. (A) ZnO nanorods grown from MnOOH seeding; (B) Cu_2O nanorods grown within a nanopore membrane templated from film shown in (A); (C) XRD analysis of Cu_2O nanorods on F-SnO_2 and the bare F-SnO_2 substrate for comparison.

dx.doi.org/10.1021/am507244q | ACS Appl. Mater. Interfaces XXXX, XXX, XXX−XXX

Supporting Information, Figures S1 and S2). Powder X-ray diffraction data indicate that the Cu_2O is polycrystalline (Figure 3C) with no predominant crystal orientation from the substrate.[19] Cu_2O having superior crystallinity, epitaxial orientation from the substrate, and higher carrier mobility can be grown at higher pH,[25,29] but we observed a breakdown of templating behavior in the growth of more crystalline Cu_2O films, so we were unable to reproducibly prepare Cu_2O nanorods above pH 9. The in situ membrane templates prepared in this new methodology are soft materials with weak surface attachment to the underlying substrate, and as a result of these characteristics, they do not confine the growth of a highly crystalline hard material such as Cu_2O. At pH higher than 9, we observed the growth of more crystalline Cu_2O with large cubic crystal grains as would be observed in the absence of any template. In early growth in poly(lactic acid) membranes at higher pH, some nanorods do form before the template is displaced by the concurrent formation of larger crystal domains (Figure S7).

We assembled photoelectrochemical cells with the Cu_2O nanorods and with planar films of electrodeposited Cu_2O to interrogate their electrical contact to the underlying F-SnO_2 electrode. We first attempted to use decamethylcobaltocene and its radical cation as the redox pair in acetonitrile, based on a report by Lewis and co-workers that demonstrated impressive photovoltage with this electrolyte.[14] However, we could not get more than 1−2 μA of photocurrent. Cu_2O is known to have surface defects that act as charge traps,[44,45] and we speculate that the polycrystalline electrodeposited Cu_2O prepared by our method is likely to have a much higher density of surface defects compared to the thermally prepared Cu_2O of their report. Such surface defects may collect electrons at electrochemical potentials below the formal conduction band edge, as known for other oxide semiconductors such as TiO_2,[46] and/or some traps may collect holes at potentials above the formal valence band edge. If surface trap states allow conduction band electrons to thermalize to more than 230 mV below the conduction band edge (−1.7 vs SCE),[12] then electron transfer to decamethylcobaltocenium (−1.47 vs SCE)[47] will be endothermic. Evaluation of the photocells using an electron shuttle with much lower redox potential can still serve to make a preliminary assessment of the photocatalytic activity of the Cu_2O nanorod films, although we may not determine their maximum photoelectrochemical potential. Previous reports have suggested that the iodide/triiodide redox couple can give good photovoltage and photocurrents with Cu_2O photocathodes. This is curious given that the redox potential of iodide/triiodide (+0.1 vs SCE)[48] is nearly isoenergetic to the Fermi level in p-type Cu_2O (+0.16 vs SCE).[1,12] It should not be possible to generate significant photocurrent with an iodide/triiodide electrolyte. Unfortunately, we were unable to adequately test this premise, as we observed instantaneous corrosion of Cu_2O films upon addition of an electrolyte composed of 0.5 M LiI and 50 mM I_2 in acetonitrile. The same result occurred with the tris(4,4′-di-*tert*-butylbipyridyl)cobalt (II/III) redox pair, for which the redox potential is ∼50 mV positive of I^-/I_3^-.[49] We chose methyl viologen to assess the photoactivity of the Cu_2O nanorods because it has a redox potential of −0.4 vs SCE and has been shown to be photoreduced in the presence of illuminated Cu_2O.[12,14,50]

We have found that the tetrafluoroborate (BF_4) salt of methyl viologen can be prepared by simple addition of aqueous HBF_4 to a suspension of the undissolved viologen dichloride salt in deionized water. This avoids the previously reported use of transition metal reagents such as $AgBF_4$ or $CuBF_4$ for salt exchange from the dichloride,[36,51] or the use of trimethyloxonium BF_4 to prepare the salt from 4,4′-bipyridine.[37] The heterogeneous salt exchange appears to be rapid upon addition of aqueous HBF_4 as judged by color change of the solid component of the mixture. Single-crystal X-ray diffraction of the water-recrystallized product indicates that no water is included in the crystal structure (Figure 4), which matches to a previous report of this compound, although we were able to obtain higher quality crystal data (see Supporting Information). To prepare a redox pair electrolyte based on methyl viologen, 0.5 mol equiv of decamethylcobaltocene was added to a 50 mM solution of the dication viologen salt in acetonitrile with 0.1 M $LiClO_4$. Upon the slow dissolution of the decamethylcobaltocene, the electrolyte turned a deep blue color (Figure 5, inset photograph). No corrosion of the Cu_2O films was observed with this electrolyte, either upon initial loading into the photocells or as a result of illumination.

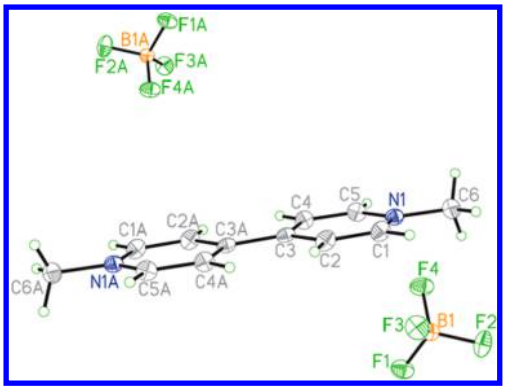

Figure 4. Crystal structure of methyl viologen tetrafluoroborate, as determined by single-crystal X-ray diffraction. The two halves of the viologen dication, as well as the two BF_4 anions, are equivalent through a center of symmetry.

The as-grown Cu_2O nanostructures exhibit an optical band gap of approximately 2.3 eV (Figure 5, top right). The photocells assembled with methyl viologen/decamethcobaltocene generate cathodic photocurrent, indicating that the Cu_2O has p-type conductivity. The external quantum efficiency measurement under back side illumination shows prominent photocurrent in a limited region from 400 to 550 nm due to the optical filtering effect of the methyl viologen radical cation in the electrolyte in the green and UV regions of the spectrum (Figure 5, left top and bottom).[50] Front side illumination, through the Cu_2O-bearing electrode, shows greater efficiency only in portions of the spectrum where the Cu_2O absorption is weaker (500−600 nm), suggesting that the Cu_2O that is farther from the electrolyte interface acts as an optical filter. Photoinduced charge separation within the Cu_2O that occurs away from the semiconductor interface leads to recombination rather than steady photocurrent. Although nanorod morphology for some semiconductors can be optimized by keeping the rod diameter wider than the depletion width but narrower than the carrier transport length,[52] we note that electrodeposited Cu_2O is not amenable to this tuning because its depletion width (∼3 μm) is much greater than its electron transport length (110 nm).[53,54] Although the morphology of Cu_2O nanorods prepared in this study does not minimize the diameter down to the carrier transport length, this may not

dx.doi.org/10.1021/am507244q | ACS Appl. Mater. Interfaces XXXX, XXX, XXX−XXX

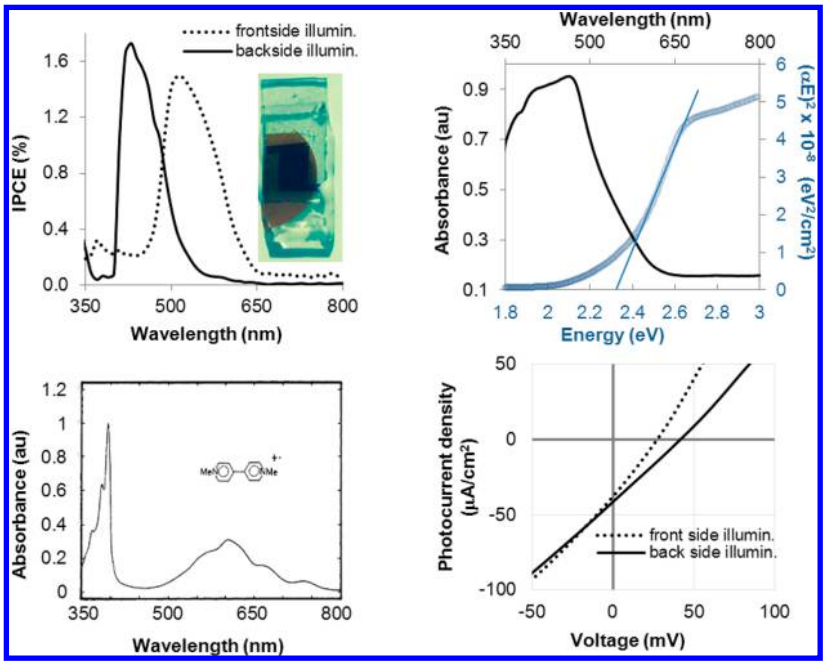

Figure 5. Clockwise from upper left: Incident photon conversion to electron (IPCE) efficiency of a photoelectrochemical cell made from a 1.2 μm film of Cu_2O nanorods on FTO glass with 50 mM methyl viologen tetrafluoroborate and 25 mM decamethylcobaltocene (cell shown in inset photo with front side up); absorbance spectrum (black) and Tauc plot (blue) for the Cu_2O nanorods film, measured prior to photocell assembly; current–voltage behavior of the photoelectrochemical cell, illuminated through the Cu_2O (front side) and through the electrolyte (backside) under AM 1.5 G light; absorbance spectrum of methyl viologen radical cation, adapted from ref 50 with permission.

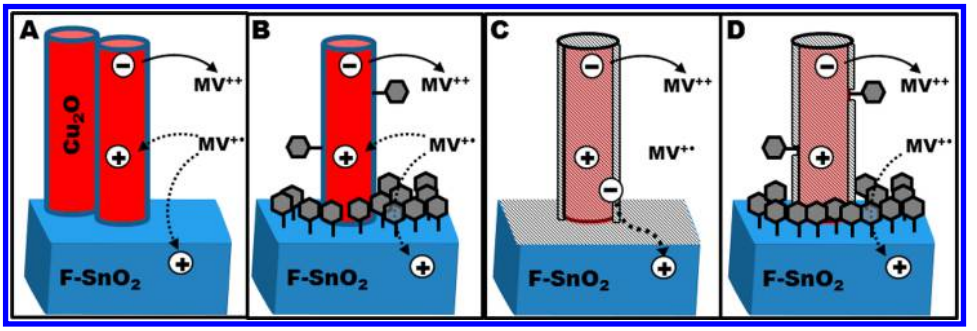

Figure 6. Interfacial recombination processes within Cu_2O photoelectrochemical cells. Solid arrows indicate forward electron transfer. Dotted arrows indicate recombination pathways. MV^{+2} is the methyl viologen dication; $MV^{+\bullet}$ is the methyl viologen radical cation (reduced form). (A) Nonpassivated cells have semiconductor/electrolyte and F-SnO_2/electrolyte recombination interfaces. (B) Cells passivated by cathodic grafting of arenediazonium salts have significant surface coverage of F-SnO_2 and possibly some Cu_2O coverage, but electron transfer is only mildly suppressed. (C) Cells passivated with amorphous TiO_2 films should have suppressed recombination involving electrolyte; however, severe recombination is expected at the TiO_2/F-SnO_2 interface. (D) Films passivated first by arenediazonium grafting and then by TiO_2 coating should suppress both the semiconductor/electrolyte and TiO_2/F-SnO_2 recombination pathways.

sufficiently explain the loss of photocurrent due to recombination because significant back electron transfer may occur at the Cu_2O/electrolyte and F-SnO_2/electrolyte interfaces (Figure 6).

Figure 6 shows the interfacial electron transfer processes in photocells using bare Cu_2O nanorods as well as for electrodes we passivated by cathodic grafting of arenediazonium salts and/or the deposition of a thin layer of amorphous TiO_2.[38,39] Surface coatings of nitrobenzene can be grafted onto electrodes using nitrobenzenediazonium tetrafluoroborate at mild cathodic potentials (−0.4–0 V vs Ag/AgCl) that should lie within the band gap of Cu_2O. The grafting mechanism is by electron transfer from the F-SnO_2 electrode to soluble arenediazonium species, liberating N_2 and creating reactive aryl radicals that then can bind to the F-SnO_2 surface. The grafting is self-limiting to only a few layers (<3 nm) because the carbonaceous coating is insufficiently conductive to facilitate the electron transfer reaction beyond a few layers of oligomerization. Although it is possible for some aryl radical molecules generated near the F-SnO_2 surface to migrate and bind to areas of the Cu_2O surface, this is unlikely due to the high reactivity of the aryl radical species. Cu_2O is known to react with diazonium reagents through Sandmeyer chemistry, and native oxide layers of Cu_2O on Cu metal have been passivated under applied potential.[55] The reduced photocurrent for a Cu_2O nanorods film subjected to diazonium grafting (Figure 7) suggests that some portion of the Cu_2O may be passivated in addition to the F-SnO_2 surface. We interpret the lack of improvement in photovoltage for diazonium-passivated cells as an indication that the oligo-aryl coatings do not significantly suppress recombination at the electrolyte/F-SnO_2 interface (Figure 6C). The planar Cu_2O films pack very densely on the

dx.doi.org/10.1021/am507244q | ACS Appl. Mater. Interfaces XXXX, XXX, XXX–XXX

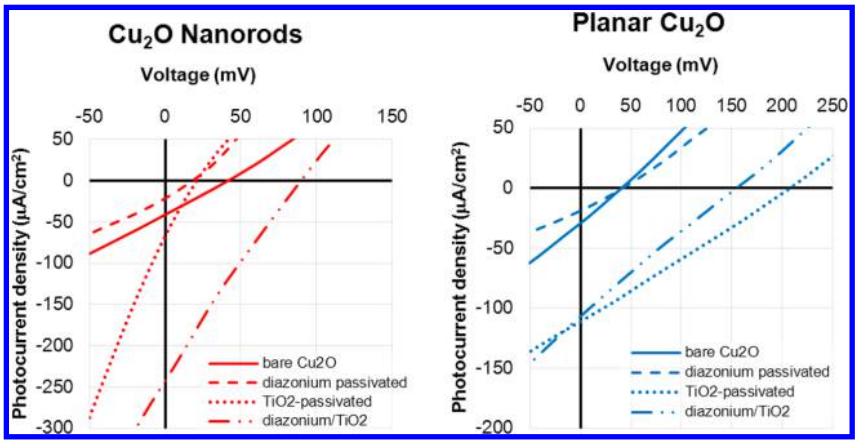

Figure 7. Current–voltage graphs of Cu_2O photoelectrochemical cells under simulated AM 1.5 G illumination. Data is shown for back side illumination only. Data for dark current and for front side illumination is shown in Supporting Information, Figures S13 and S14.

surface[19,20] (see Supporting Information), occluding the F-SnO_2 surface, and photocells made from planar Cu_2O films showed better photovoltage under each of the preparation conditions compared to the Cu_2O nanorod films.

We next attempted to suppress the Cu_2O/electrolyte recombination by passivating the Cu_2O surface with a thin layer of TiO_2, following a report by Gratzel and co-workers that showed improvement in the water reduction at TiO_2-passivated Cu_2O films.[56] Whereas the earlier report utilized atomic layer deposition to deposit TiO_2 as a surface coating, we have exploited the liquid phase deposition of a TiO_2 coating via the hydrolytic decomposition of ammonium hexafluorotitanate in aqueous boric acid.[39] Boric acid acts as a fluoride scavenger to drive the hydrolysis of the hexafluorotitanate to TiO_2, and the nascent metal oxide clusters/nanoparticles that form in the aqueous solution are attracted to high dielectric surfaces. TiO_2 precipitation in solution is not observed. TiO_2-coated Cu_2O appears by visual observation to have a colorless coating; however, the coating was too thin for the TiO_2 to be detected in XRD analysis of a coated film (see Supporting Information). Unfortunately, in covering both the Cu_2O and the F-SnO_2 surfaces, the TiO_2 coating creates a recombination pathway between the two, replacing the Cu_2O/electrolyte and F-SnO_2/electrolyte recombination interfaces with a TiO_2/F-SnO_2 interface. Thus, the TiO_2 coating on the Cu_2O nanorods film shows barely any improvement in photocurrent and a loss of photovoltage. The planar Cu_2O film, which has very little exposed F-SnO_2 surface, is greatly enhanced by the TiO_2 coating, showing that this Cu_2O/TiO_2 surface bilayer does improve the balance of forward/backward electron transfer at the semiconductor/electrolyte interface in the absence of other recombination avenues.

Since the TiO_2 coating occurs at high dielectric surfaces, we attempted to selectively coat the Cu_2O by first passivating the F-SnO_2 via the diazonium grafting to render those sites hydrophobic and prevent TiO_2 deposition. This dual passivation provides a sixfold increase in photocurrent for passivated versus bare Cu_2O nanorod devices, reaching 240 $\mu A/cm^2$ at short circuit. Although some areas of the Cu_2O are likely passivated by the diazonium grafting as well, the improved photocurrent indicates that the selective coating of the TiO_2 over only the Cu_2O surface is effective in suppressing recombination at the Cu_2O/electrolyte interface without providing a new TiO_2/F-SnO_2 recombination pathway. In contrast, the planar Cu_2O film was hindered by the dual passivation: since there are few exposed F-SnO_2 surfaces, selective TiO_2 coating is not important to the overall forward/backward electron transfer, so the partial passivation of the Cu_2O surface does some harm to the device performance, with no concomitant benefit. Here we see that the higher surface area of the nanorods morphology can enable increased photocurrent. Photovoltage in the planar films is still better than even the dual-passivated nanorods device, which shows that interfacial recombination is still a significant limiting factor on device performance for Cu_2O nanorod films, and more effective passivation methods are needed to further enhance the photoelectrochemical behavior.

CONCLUSIONS

We have observed the highest photocurrent ever reported for an electrodeposited Cu_2O film in a nonaqueous photoelectrochemical cell. This result supports the premise that the higher surface area of nanostructured materials can enhance interfacial electron transfer for this p-type semiconductor. Results from attempts to passivate the electrolyte interfaces indicate that further enhancements in photocurrent and photovoltage are possible for nanostructured Cu_2O films, and changes in the morphology of the ZnO nanorods template can enable the preparation of morphology with diameters closer to the electron diffusion length to minimize the internal charge recombination in the semiconductor. There is a need for a different electrolyte with redox potential that is less positive of the TiO_2 conduction band edge and has weaker light absorption in the visible spectrum. As an alternative to passivating the Cu_2O surface with an n-type metal oxide semiconductor, molecular dyes, especially those that absorb light in the red portion of the visible spectrum, may suppress the back electron transfer at the Cu_2O electrolyte while also contributing to photocurrent. The field of p-type dye-sensitized solar cells is still greatly in need of new nanostructured intrinsic p-type semiconductor photocathode materials.[57] As a final observation, we note that the general method we have reported herein for templating the preparation of epitaxially oriented Cu_2O nanorods from ZnO precursor films may also serve for the electrodeposition of films of other materials on preformed electrode substrates that are difficult to prepare in this morphology.

■ ASSOCIATED CONTENT

Supporting Information

Additional SEM images of prepared nanorod films, powder and single-crystal X-ray diffraction data, and additional photoelectrochemical characterization data. This material is available free of charge via the Internet at http://pubs.acs.org.

■ AUTHOR INFORMATION

Corresponding Author

*E-mail: youngblood@unt.edu.

Notes

The authors declare no competing financial interest.

■ ACKNOWLEDGMENTS

We thank the UNT Center for Advanced Research and Technology (CART) for an instrument usage grant to obtain SEM and profilometry measurements, the University of North Texas for start-up funding, and the National Science Foundation (NSF-REU support for M.R. under Grant CHE-1004878).

■ REFERENCES

(1) Assimos, J. A.; Trivich, D. The Photoelectric Threshold, Work Function, and Surface Barrier Potential of Single-Crystal Cuprous Oxide. *Phys. Status Solidi* **1974**, *26*, 477−488.

(2) Nolan, M.; Elliott, S. D. The p-Type Conduction Mechanism in Cu_2O: A First Principles Study. *Phys. Chem. Chem. Phys.* **2006**, *8*, 5350−5358.

(3) Raebiger, H.; Lany, S.; Zunger, A. Origins of the *p*-Type Nature and Cation Deficiency in Cu_2O and Related Materials. *Phys. Rev. B* **2007**, *76*, 045209.

(4) Scanlon, D. O.; Morgan, B. J.; Watson, G. W.; Walsh, A. Acceptor Levels in p-Type Cu_2O: Rationalizing Theory and Experiment. *Phys. Rev. Lett.* **2009**, *103*, 096405.

(5) Zhang, J.; Liu, J.; Peng, Q.; Wang, X.; Li, Y. Nearly Monodisperse Cu_2O and CuO Nanospheres: Preparation and Applications for Sensitive Gas Sensors. *Chem. Mater.* **2006**, *18*, 867−871.

(6) Deng, S.; Tjoa, V.; Fan, H. M.; Tan, H. R.; Sayle, D. C.; Olivo, M.; Mhaisalkar, S.; Wei, J.; Sow, C. H. Reduced Graphene Oxide Conjugated Cu_2O Nanowire Mesocrystals for High-Performance NO_2 Gas Sensor. *J. Am. Chem. Soc.* **2012**, *134*, 4905−4917.

(7) Garrison, A. The Photo-Chemical Properties of Cuprous Oxide. *J. Phys. Chem.* **1924**, *28*, 279−284.

(8) Hara, M.; Kondo, T.; Komoda, M.; Ikeda, S.; Shinohara, K.; Tanaka, A.; Kondo, J. N.; Domen, K. Cu_2O as a Photocatalyst for Overall Water Splitting Under Visible Light Irradiation. *Chem. Commun.* **1998**, 357−358.

(9) Garrison, A. The Behavior of Cuprous Oxide Photo-Voltaic Cells. *J. Phys. Chem.* **1923**, *27*, 601−622.

(10) Rai, B. P. Cu_2O Solar Cells: A Review. *Sol. Cells* **1988**, *25*, 265−272.

(11) Briskman, R. N. A Study of Electrodeposited Cuprous Oxide Photovoltaic Cells. *Sol. Energy. Mater. Sol. Cells* **1992**, *27*, 361−368.

(12) Nagasubramanian, G.; Gioda, A. S.; Bard, A. J. Semiconductor Electrodes XXXVII. Photoelectrochemical Behavior of p-Type Cu_2O in Acetonitrile Solutions. *J. Electrochem. Soc.* **1981**, *128*, 2158−2164.

(13) Sculfort, J. L.; Guyomard, D.; Herlem, M. Photoelectrochemical Characterization of the p-Cu_2O-Non Aqueous Electrolyte Junction. *Electrochim. Acta* **1984**, *29*, 459−465.

(14) Xiang, C.; Kimball, G. M.; Grimm, R. L.; Brunschwig, B. S.; Atwater, H. A.; Lewis, N. S. 820 mV open-circuit voltages from Cu_2O/CH_3CN junctions. *Energy Environ. Sci.* **2011**, *4*, 1311−1318.

(15) Gerischer, H. On The Stability Of Semiconductor Electrodes Against Photodecomposition. *J. Electroanal. Chem.* **1977**, *82*, 133−143.

(16) Wu, L.; Tsui, L.; Swami, N.; Zangari, G. Photoelectrochemical Stability of Electrodeposited Cu_2O Films. *J. Phys. Chem. C* **2010**, *114*, 11551−11556.

(17) Olsen, L. C.; Bohara, R. C.; Urie, M. W. Explanation for Low Efficiency Cu_2O Schottky Barrier Solar Cells. *Appl. Phys. Lett.* **1979**, *34*, 47−49.

(18) Olsen, L. C.; Addis, F. W.; Miller, W. Experimental and Theoretical Studies of Cu_2O Solar Cells. *Sol. Cells* **1982**, *7*, 247−279.

(19) Golden, T. D.; Shumsky, M. G.; Zhou, Y.; VanderWerf, R. A.; Van Leeuwen, R. A.; Switzer, J. A. Electrochemical Deposition of Copper (I) Oxide Films. *Chem. Mater.* **1996**, *8*, 2499−2504.

(20) de Jongh, P. E.; Vanmaekelbergh, D.; Kelly, J. J. Cu_2O: Electrodeposition and Characterization. *Chem. Mater.* **1999**, *11*, 3512−3517.

(21) Siegfried, M.; Choi, K.-S. Electrochemical Crystallization of Cuprous Oxide with Systematic Shape Evolution. *Adv. Mater.* **2004**, *16*, 1743−1746.

(22) Brown, K. E. R.; Choi, K.-S. Electrochemical Synthesis and Characterization of Transparent Nanocrystalline Cu_2O Films and Their Conversion to CuO Films. *Chem. Commun.* **2006**, 3311−3313.

(23) Wang, W.; Wu, D.; Zhang, Q.; Wang, L.; Tao, M. pH-Dependence of Conduction Type in Cuprous Oxide Synthesized from Solution. *J. Appl. Phys.* **2010**, *107*, 123717.

(24) Haller, S.; Jung, J.; Rousset, J.; Lincot, D. Effect of Electrodeposition Parameters and Addition of Chloride Ions on the Structural and Optoelectronic Properties of Cu_2O. *Electrochim. Acta* **2012**, *82*, 402−407.

(25) Septina, W.; Ikeda, S.; Khan, M. A.; Hirai, T.; Harada, T.; Matsumura, M.; Peter, L. M. Potentiostatic Electrodeposition of Cuprous Oxide Thin Films for Photovoltaic Applications. *Electrochim. Acta* **2011**, *56*, 4882−4888.

(26) Osherov, A.; Zhu, C.; Panzer, M. J. Role of Solution Chemistry in Determining the Morphology and Photoconductivity of Electrodeposited Cuprous Oxide Films. *Chem. Mater.* **2013**, *25*, 692−698.

(27) Paracchino, A.; Brauer, J. C.; Moser, J.-E.; Thimsen, E.; Graetzel, M. Synthesis and Characterization of High-Photoactivity Electrodeposited Cu_2O Solar Absorber by Photoelectrochemistry and Ultrafast Spectroscopy. *J. Phys. Chem. C* **2012**, *116*, 7341−7350.

(28) Mahalingam, T.; Chitra, J. S. P.; Chu, J. P.; Velumani, S.; Sebastian, P. J. Structural and Annealing Studies of Potentiostatically Deposited Cu_2O Thin Films. *Sol. Energy Mater. Sol. Cells* **2005**, *88*, 209−216.

(29) Mizuno, K.; Izaki, M.; Murase, K.; Shinagawa, T.; Chigane, M.; Inaba, M.; Tasaka, A.; Awakura, Y. Structural and Electrical Characterizations of Electrodeposited p-Type Semiconductor Cu_2O Films. *J. Electrochem. Soc.* **2005**, *152*, C179−C182.

(30) Poulston, S.; Parlett, P. M.; Stone, P.; Bowker, M. Surface Oxidation and Reduction of CuO and Cu_2O Studied Using XPS and XAES. *Surf. Interface Anal.* **1996**, *24*, 811−820.

(31) Yuhas, B. D.; Yang, P. Nanowire-Based All-Oxide Solar Cells. *J. Am. Chem. Soc.* **2009**, *131*, 3756−3761.

(32) Kokotov, M.; Hodes, G. Reliable Chemical Bath Depostion of ZnO Films With Controllable Morphology From Ethanolamine-Based Solutions Using $KMnO_4$ Substrate Activation. *J. Mater. Chem.* **2009**, *19*, 3847−3854.

(33) Rodríguez, J.; Paraguay-Delgado, F.; Lopez, A.; Alarcon, J.; Estrada, W. Synthesis and Characterization of ZnO Nanorod Films for Photocatalytic Disinfection of Contaminated Water. *Thin Solid Films* **2010**, *519*, 729−735.

(34) Bergfield, W. F.; Belsito, D. V.; Hill, R. A.; Klaasen, C. D.; Liebler, D. C.; Marks, Jr., J. G.; Shank, R. C.; Slaga, T. J.; Snyder, P. W. *Safety Assessment of Nitrocellulose as Used in Cosmetics*; Cosmetic Ingredient Review: Washington, D.C., 2013.

(35) Papageorgiou, N.; Maier, W. F.; Gratzel, M. An Iodine/Triiodide Reduction Electrocatalyst for Aqueous and Organic Media. *J. Electrochem. Soc.* **1997**, *144*, 876−884.

(36) Yang, F.; Deng, J.-C.; Li, Z.-G.; Xu, J.-W. 1,1′-Dimethyl-4,4″-bipyridinium bis(tetrafluoridoborate). *Acta Crystallogr.* **2008**, *E64*, o253.

(37) Mori, T.; Inoue, Y.; Grimme, S. Experimental and Theoretical Study of the CD Spectra and Conformational Properties of Axially Chiral 2,2′-, 3,3′-, and 4,4′-Biphenol Ethers. *J. Phys. Chem. A* **2007**, *111*, 4222−4234.
(38) Maldonado, S.; Smith, T. J.; William, R. D.; Morin, S.; Barton, E.; Stevenson, K. J. Surface Modification of Indium Tin Oxide via Electrochemical Reduction of Aryldiazonium Cations. *Langmuir* **2006**, *22*, 2884−2891.
(39) Lee, J.-H.; Leu, I.-C.; Hsu, M.-C.; Chung, Y.-W.; Hon, M.-H. Fabrication of Aligned TiO_2 One-Dimensional Nanostructured Arrays Using a One-Step Templating Solution Approach. *J. Phys. Chem. B* **2005**, *109*, 13056−13059.
(40) Gonzales-Valls, I.; Lira-Cantu, M. Vertically Aligned Nanostructures of ZnO for Excitonic Solar Cells: A Review. *Energy Environ.* **2009**, *2*, 19−34.
(41) Gou, L.; Murphy, C. J. Solution-Phase Synthesis of Cu_2O Nanocubes. *Nano Lett.* **2003**, *3*, 231−234.
(42) Xu, H.; Wang, W.; Zhu, W. Shape Evolution and Size-Controllable Synthesis of Cu2O Octahedra and Their Morphology-Dependent Photocatalytic Properties. *J. Phys. Chem. B* **2006**, *110*, 13829−13834.
(43) Kuo, C.-H.; Huang, M. H. Facile Synthesis of Cu_2O Nanocrystals with Systematic Shape Evolution from Cubic to Octahedral Structures. *J. Phys. Chem. C* **2008**, *112*, 18355−18360.
(44) Ishizuka, S.; Kato, S.; Okamoto, Y.; Sakurai, T.; Akimoto, K.; Fujiwara, N.; Kobayashi, H. Passivation of Defects in Polycrystalline Cu_2O Thin Films by Hydrogen or Cyanide Treatment. *Appl. Surf. Sci.* **2003**, *216*, 94−97.
(45) Paul, G. K.; Ghosh, R.; Bera, S. K.; Bandyopadhyay, S.; Sakurai, T.; Akimoto, K. Deep Level Transient Spectroscopy of Cyanide Treated Polycrystalline p-Cu_2O/n-ZnO Solar Cell. *Chem. Phys. Lett.* **2008**, *463*, 117−120.
(46) van de Lagemaat, J.; Frank, A. J. Nonthermalized Electron Transport in Dye-Sensitized Nanocrystalline TiO_2 Films: Transient Photocurrent and Random-Walk Modeling Studies. *J. Phys. Chem. B* **2001**, *105*, 11194−11205.
(47) Robbins, J. L.; Edelstein, N.; Spencer, B.; Smart, J. C. Syntheses and Electronic Structures of Decamethylmetallocenes. *J. Am. Chem. Soc.* **1982**, *104*, 1882−1893.
(48) Gibson, E. A.; Smeigh, A. L.; Le Pleux, L.; Hammarström, L.; Odobel, F.; Boschloo, G.; Hagfeldt, A. Cobalt Polypyridyl-Based Electrolytes for p-Type Dye-Sensitized Solar Cells. *J. Phys. Chem. C* **2011**, *115*, 9772−9779.
(49) Sapp, S. A.; Elliott, C. M.; Contado, C.; Caramori, S.; Bignozzi, C. A. Substituted Polypyridine Complexes of Cobalt(II/III) as Efficient Electron-Transfer Mediators in Dye-Sensitized Solar Cells. *J. Am. Chem. Soc.* **2001**, *124*, 11215−11222.
(50) Bockman, T. M.; Kochi, J. K. Isolation and Oxidation-Reduction of Methylviologen Cation Radicals. Novel Disproportionation in Charge-Transfer Salts by X-ray Crystallography. *J. Org. Chem.* **1990**, *55*, 4127−4135.
(51) Peon, J.; Tan, X.; Hoerner, D.; Xia, C.; Luk, Y. F.; Kohler, B. Excited State Dynamics of Methyl Viologen. Ultrafast Photoreduction in Methanol and Fluorescence in Acetonitrile. *J. Phys. Chem. A* **2001**, *105*, 5768−5777.
(52) Hagedorn, K.; Forgacs, C.; Collins, S.; Maldonado, S. Design Considerations for Nanowire Heterojunctions in Solar Energy Conversion/Storage Applications. *J. Phys. Chem. C* **2010**, *114*, 12010−12017.
(53) Musselman, K. P.; Marin, A.; Schmidt-Mende, L.; MacManus-Driscoll, J. L. Incompatible Length Scales in Nanostructured Cu_2O Solar Cells. *Adv. Funct. Mater.* **2012**, *22*, 2202−2208.
(54) Musselman, K. P.; Ievskaya, Y.; MacManus-Driscoll, J. L. Modelling Charge Transport Lengths in Heterojunction Solar Cells. *Appl. Phys. Lett.* **2012**, *101*, 253503.
(55) Hurley, B. L.; McCreery, R. L. Covalent Bonding of Organic Molecules to Cu and Al Alloy 2024 T3 Surfaces via Diazonium Ion Reduction. *J. Electrochem. Soc.* **2004**, *151*, B252−B259.
(56) Paracchino, A.; Laporte, V.; Sivula, K.; Gratzel, M.; Thimsen, E. Highly Active Oxide Photocathode for Photoelectrochemical Water Reduction. *Nat. Mater.* **2011**, *10*, 456−461.
(57) Odobel, F.; Le Pleux, L.; Pellegrin, Y.; Blart, E. New Photovoltaic Devices Based on the Sensitization of p-type Semiconductors: Challenges and Opportunities. *Acc. Chem. Res.* **2010**, *34*, 1063−1071.